A ZnO microcantilever for high-frequency nanopositioning : modeling, fabrication and characterization

Yuan, Yanhui; Du, Hejun; Wang, Peihong; Chow, Kun Shyong; Zhang, Mingsheng; Yu, Shengkai; Liu, Bo

2013

Yuan, Y., Du, H., Wang, P., Chow, K. S., Zhang, M., Yu, S., et al. (2013). A ZnO microcantilever for high-frequency nanopositioning: Modeling, fabrication and characterization. Sensors and Actuators A: Physical, 194, 75-83.

https://hdl.handle.net/10356/101399

https://doi.org/10.1016/j.sna.2013.02.002

A ZnO microcantilever for high-frequency nanopositioning: modeling, fabrication and characterization

Yanhui Yuan[a], **Hejun Du**[a,*], **Peihong Wang**[a], **Kun Shyong Chow**[a], **Mingsheng Zhang**[b], **Shengkai Yu**[b], **Bo Liu**[b]
[a]*School of Mechanical and Aerospace Engineering, Nanyang Technological University, 639798, Singapore*
[b]*Data Storage Institute, 117608, Singapore*

Abstract
Previous studies on zinc oxide (ZnO) microcantilevers have been focused on applications in the atomic force microscopy (AFM). Characteristics of ZnO microcantilever actuators were not thoroughly investigated in those studies. This paper reports modeling, fabrication and characterization of a piezoelectric ZnO microcantilever actuator for high-frequency nanopositioning. Main characteristics of the ZnO microcantilever, i.e. resonant frequency, actuation sensitivity and force-deflection relationship, have been studied by modeling and experiments. Analytic equations of the resonant frequency and actuation sensitivity were derived. Tip deflection as a function of driving voltage and external load was formulated. Effects of major geometric dimensions on the performance of piezoelectric ZnO cantilevers were demonstrated with numerical results. A prototype was designed for applications requiring micro-Newton actuation forces with driving frequencies above 10 kHz. The microfabricated cantilever was characterized for its resonant frequency and actuation sensitivity. Impedance analysis identified the resonant frequency at 53 kHz which was in excellent agreement with the frequency response function. Steady-state actuation sensitivity at 15 kHz was found to be 12 nm/V with a bandwidth of 27 kHz.

Keywords: ZnO; thin film; microcantilever; nanopositioning

[*] Corresponding author. Tel: +65 6790 4783; Fax: +65 6790 4783; Email address: mhdu@ntu.edu.sg

1. Introduction

Piezoelectric cantilever actuators utilize the converse piezoelectric effect to convert electrical energy into mechanical energy, i.e. displacement and force. Typical applications of piezoelectric cantilever actuators include ultrasonic motors, atomic-force-microscopy (AFM) probes, microwave switches, bandpass filters and suspensions in hard disk drives [1-5].

Among the broad range of piezoelectric materials, lead zirconate titanate (PZT) is the most widely used due to its superior piezoelectricity. Apart from PZT, zinc oxide (ZnO) is another important piezoelectric material. Although piezoelectricity of ZnO is generally one order smaller than that of PZT [6], ZnO possesses greater flexibility in processing. ZnO thin films can be deposited in room temperature and easily etched by a variety of acidic etchants [7]. Therefore, it can be readily integrated with other MEMS materials and processes.

Most of previous works on ZnO cantilever actuators were related to the AFM. A ZnO cantilever was first used as a sensor to overcome limitations of conventional photo detectors in the AFM [8, 9]. In attempts for further improvements, actuation capability was added to the cantilever with double ZnO layers to realize self-excitation [10, 11]. In a similar application, a ZnO thin film was implemented on the cantilever to enhance the scanning speed of the AFM [12, 13]. These studies were mainly focused on improving performance of the AFM. Preparation of the ZnO thin film and the characteristics of the ZnO actuator were not thoroughly studied. Later efforts were concerned more with characterization of ZnO cantilevers. In [14], a method for calculation of the transverse piezoelectric constant based on the free vibration theory of a cantilever beam was proposed. In another study, higher vibration modes of a commercial ZnO cantilever were investigated using impedance analysis [15]. The nonlinear behaviour of a similar cantilever was demonstrated by theoretical development and experimental results [16]. Although the aforementioned characterization efforts addressed some issues regarding characteristics of ZnO cantilevers, two most important aspects, i.e. actuation sensitivity and force-deflection behaviour, were neglected.

This paper reports a systematic study on a ZnO microcantilever for high-frequency nanopositioning. The microcantilever was designed to operate in the frequency range of up to 20 kHz. The tip deflection was on the order of a few nanometers with actuation force on the micro-Newton level. Modeling of the microcantilever concerning its resonant frequency, force-deflection relationship and actuation sensitivity will be first presented. Fabrication processes including preparation of thin-film ZnO by RF magnetron sputtering and micromachining of the cantilever will then be described in detail. Lastly, characterization results of the resonant frequency and actuation sensitivity will be discussed and compared with theoretical values.

2. Modeling and design

Two common approaches have been used in existing studies to derive the constitutive equations of piezoelectric cantilever benders. The first approach is to consider equilibrium of forces and moments and the strain compatibility condition at the piezoelectric-elastic interface [17, 18]. This approach was first proposed by S. Timoshenko for analysis of bimetallic thermostats [19]. Usually, tip deflection of an unloaded piezoelectric cantilever is first calculated based on the curvature. Actuation force can then be obtained by utilizing the equivalent force-deflection relationship at the tip of the cantilever. The second approach is based on the energy method which involves calculation of strain energy and piezoelectric energy [20, 21]. This paper follows the first approach and starts with a loaded cantilever. Bending moment instead of the curvature is then derived. By integration of the bending-moment equation, an integrated governing equation for tip deflection, external loading and driving electric field is obtained.

As shown in Fig. 1(a), a piezoelectric cantilever is commonly used to displace an external load P by a certain displacement δ. In addition to loading and displacement, the speed of positioning also has to meet the requirements of specific applications. Thus, the resonant frequency and force-displacement relationship are the most concerned specifications in the design of piezoelectric cantilever actuators.

2.1. Bending resonant frequency

Free bending vibration of beams is governed by a fourth-order partial differential equation which can be solved by separation of variables in space and time. The resonant frequencies can be obtained by solving the eigenvalue problem of the fourth-order ordinary differential equation in space. The fundamental resonant frequency ω_0 of a beam clamped at one end and free at the other end is given by [22]

$$\omega_0 = 3.5160\sqrt{\frac{EI}{mL^4}} \tag{1}$$

where *E*, *I*, *m* and *L* are the Young's modulus, area moment of inertia, mass per unit length and length of the beam, respectively. To find the flexural rigidity *EI* for the piezoelectric cantilever which consists of two materials, the transformed-section method is used to transform its cross section into an equivalent cross section of a single material [23]. The equivalent flexural rigidity *EI* is found to be

$$EI = \frac{b\beta}{12(E_p t_p + E_s t_s)} \tag{2}$$

where the subscripts *p* and *s* denote the piezoelectric and elastic materials, respectively; and *b*, *t* are the width and thickness, respectively. And, β represents

$$\beta = E_p^2 t_p^4 + E_s^2 t_s^4 + 4E_p E_s t_s t_p^3 + 4E_p E_s t_p t_s^3 + 6E_p E_s t_p^2 t_s^2 \tag{3}$$

The equivalent mass per unit length *m* for the piezoelectric cantilever is

$$m = b(t_p \rho_p + t_s \rho_s) \tag{4}$$

where ρ is density. Insertion of Eqs. (2), (4) and $f_0 = \omega_0 / 2\pi$ into Eq. (1) gives the resonant frequency f_0,

$$f_0 = \frac{0.1615}{L^2}\sqrt{\frac{\beta}{(E_p t_p + E_s t_s)(t_p \rho_p + t_s \rho_s)}} \tag{5}$$

2.2. Tip deflection and actuation force

Similar to the effect of temperature change on bimetallic thermostats, an electric field induces internal stress in the piezoelectric cantilever. The stress at an arbitrary cross section can be represented by axial forces and internal moments [19]. Fig. 1(b) is a free-body diagram of a segment along the length of the piezoelectric cantilever actuator. Equilibrium conditions of force and moment on any cross section of the cantilever are

$$F_p = F_s \tag{6}$$

$$\frac{F_p t_p}{2} + \frac{F_s t_s}{2} = M_p + M_s \tag{7}$$

According to the moment-curvature equation [23], the moments M_p and M_s can be expressed in terms of the curvature *r* of the cantilever as follows,

$$M_p = \frac{E_p I_p}{r} \tag{8}$$

$$M_s = \frac{E_s I_s}{r} \tag{9}$$

Combining Eqs. (8) and (9) gives

$$\frac{M_p}{M_s} = \frac{E_p I_p}{E_s I_s} \tag{10}$$

Upon substitution of $I_p = \frac{bt_p^3}{12}$ and $I_s = \frac{bt_s^3}{12}$, Eq. (10) becomes

$$\frac{M_p}{M_s} = \frac{E_p t_p^3}{E_s t_s^3} \tag{11}$$

Assuming there is no separation and slip at the interface of the piezoelectric and elastic layers, the normal strain in the piezoelectric layer must be equal to that in the elastic layer. Therefore,

$$-d_{31}E_3 + \frac{F_p}{E_p t_p b} + \frac{M_p t_p}{2E_p I_p} = -\frac{F_s}{E_s t_s b} - \frac{M_s t_s}{2E_s I_s} \tag{12}$$

where d_{31} and E_3 are the transverse piezoelectric constant and electric filed across the thickness of the piezoelectric layer, respectively. Upon substitution of $I_p = \frac{bt_p^3}{12}$ and $I_s = \frac{bt_s^3}{12}$, Eq. (12) becomes

$$-d_{31}E_3 + \frac{F_p}{E_p t_p b} + \frac{6M_p}{E_p b t_p^2} = -\frac{F_s}{E_s t_s b} - \frac{6M_s}{E_s b t_s^2} \tag{13}$$

The forces and moments, i.e. F_p, F_s, M_p, and M_s can be derived by solving Eqs. (6), (7), (11) and (13). M_p and M_s are found as follows,

$$M_p = \frac{bd_{31}E_3E_p^2E_s t_p^4 t_s(t_p + t_s)}{2\beta} \tag{14}$$

$$M_s = \frac{bd_{31}E_3E_pE_s^2 t_p t_s^4(t_p + t_s)}{2\beta} \tag{15}$$

Summation of M_p from Eq. (14) and M_s from Eq. (15) gives the bending moment M_E induced by the electric field,

$$M_E = \frac{bd_{31}E_3E_pE_s t_p t_s(t_p + t_s)(E_p t_p^3 + E_s t_s^3)}{2\beta} \tag{16}$$

In addition to the electric field, the external load P also causes a bending moment in the cantilever which is a function of x. Thus, the total bending moment in a cross section located at x along the beam is

$$M = \frac{bd_{31}E_3E_pE_s t_p t_s(t_p + t_s)(E_p t_p^3 + E_s t_s^3)}{2\beta} - P(L - x) \tag{17}$$

After the moment is obtained, the deflection curve of the beam can be found by integration of the bending-moment equation. The bending-moment equation is given by [23]

$$\frac{d^2v}{dx^2} = \frac{M}{EI} \tag{18}$$

where v is deflection of the cantilever. Two integrations are required to obtain the deflection curve. Upon substitution of Eq. (17), integration of Eq. (18) produces the slope $v' = dv/dx$,

$$v' = \frac{1}{EI}\left[\frac{bd_{31}E_3E_pE_s t_p t_s(t_p + t_s)(E_p t_p^3 + E_s t_s^3)}{2\beta} - PL\right]x + \frac{1}{2EI}Px^2 + c_1 \tag{19}$$

Consideration of the first boundary condition $v' = 0$ for $x = 0$ gives $c_1 = 0$. Thus, Eq. (19) becomes

$$v' = \frac{1}{EI}\left[\frac{bd_{31}E_3E_pE_s t_p t_s(t_p + t_s)(E_p t_p^3 + E_s t_s^3)}{2\beta} - PL\right]x + \frac{1}{2EI}Px^2 \tag{20}$$

Integration of Eq. (20) gives the deflection curve,

$$v = \frac{1}{EI}\left\{\left[\frac{bd_{31}E_3E_pE_s t_p t_s(t_p + t_s)(E_p t_p^3 + E_s t_s^3)}{4\beta} - \frac{PL}{2}\right]x^2 + \frac{Px^3}{6}\right\} + c_2 \tag{21}$$

Again the second boundary condition $v = 0$ for $x = 0$ gives $c_2 = 0$. Thus,

$$v = \frac{1}{EI}\left\{\left[\frac{bd_{31}E_3E_pE_st_pt_s(t_p+t_s)(E_pt_p^3+E_st_s^3)}{4\beta} - \frac{PL}{2}\right]x^2 + \frac{Px^3}{6}\right\} \tag{22}$$

Substitutions of EI from Eq. (2) and $E_3 = V/t_p$ into Eq. (22) yield

$$v = \frac{3d_{31}VE_pE_st_s(t_p+t_s)(E_pt_p+E_st_s)(E_pt_p^3+E_st_s^3)x^2}{\beta^2} - \frac{4P(E_pt_p+E_st_s)x^3}{b\beta} \tag{23}$$

The tip deflection δ is found by substitution of $x = L$ into Eq. (23),

$$\delta = \frac{3d_{31}VE_pE_st_s(t_p+t_s)(E_pt_p+E_st_s)(E_pt_p^3+E_st_s^3)L^2}{\beta^2} - \frac{4P(E_pt_p+E_st_s)L^3}{b\beta} \tag{24}$$

2.3. Actuation sensitivity

The actuation sensitivity of an unloaded actuator can be defined either as tip deflection per voltage (δ/V) or tip deflection per electric field (δ/E_3). Tip deflection per voltage (δ/V) can be obtained from Eq. (24),

$$\frac{\delta}{V} = \frac{3d_{31}E_pE_st_s(t_p+t_s)(E_pt_p+E_st_s)(E_pt_p^3+E_st_s^3)L^2}{\beta^2} \tag{25}$$

Substitution of $V = E_3t_p$ into Eq. (25) gives tip deflection per electric field (δ/E_3),

$$\frac{\delta}{E_3} = \frac{3d_{31}E_pE_st_pt_s(t_p+t_s)(E_pt_p+E_st_s)(E_pt_p^3+E_st_s^3)L^2}{\beta^2} \tag{26}$$

2.4. Performance analysis

The resonant frequency f_0 and tip deflection δ are functions of the dimensions of the piezoelectric cantilever. As shown in Eqs. (5) and (24), the width b does not affect the resonant frequency and the tip deflection under no external loading. Considering the external load P, the driving voltage required for a certain tip deflection δ is inversely proportional to the width b. Thus, a wider cross section of the piezoelectric cantilever is preferred for less power consumption. The effect of length L can be easily seen from Eqs. (5) and (24). The resonant frequency decreases parabolically with L, while the tip deflection increases parabolically with L for $P = 0$. The effect of the thicknesses t_p and t_s is not obvious and can be studied with numerical analysis. In the following numerical and experimental results, silicon is used as the material for the elastic layer and ZnO for the piezoelectric layer. The material properties of ZnO and silicon [24, 25] are listed in Table 1.

The effect of silicon thickness on the resonant frequency and sensitivities was calculated with the ZnO thickness t_p set to 1 μm. As seen in Fig. 2, the resonant frequency f_0 increases almost linearly with the silicon thickness t_s, while the sensitivities (δ/E_3 and δ/V) both decrease parabolically with t_s. This shows the well-known trade-off between the resonant frequency and sensitivity of cantilevered transducers. It is also observed in Fig. 2(b) and Fig. 2(c) that δ/E_3 and δ/V have the same decreasing trend. This is due to the fact that the ZnO thickness t_p is fixed and $V = E_3t_p$.

Some applications such as piezoelectric actuators fabricated using the Reduced and INternally Biased Oxide Wafer (RAINBOW) require a fixed total thickness [26]. In this case, performance of the actuator changes with the thickness ratio of the elastic layer to the piezoelectric layer. Fig. 3 shows the resonant frequency and actuation sensitivity (δ/E_3, δ/V) with the total thickness set to 35 μm. It can be seen from Fig. 3(a) that f_0 increases with the thickness of silicon t_s. This is mainly caused by the decrease in density (Table 1) and thus total mass. The tip deflection under unit electric field (Fig. 3(b)) peaks at $t_s = 28$ μm, while the tip deflection under unit voltage (Fig. 3(c)) increases monotonously. The parabolic behavior of δ/E_3 in Eq. (26) is caused by the parameter t_p introduced by $V = E_3t_p$ into Eq. (25). In practice, the actuation sensitivity is primarily defined as the tip deflection per voltage (δ/V). One disadvantage of the definition of δ/V is that it is not able to reflect the physical limits of the thickness of the piezoelectric layer

and the electric field. According to Eq. (25), the thickness of the piezoelectric layer t_p can be zero. In reality, the tip deflection as well as the sensitivity δ/V shall also be zero when no piezoelectric material is present. However, the sensitivity reaches the maximum for t_p = 0 μm and t_s = 35 μm in Fig. 3(c). By contrast, δ/E_3 (Eq. 26) approaches zero with t_p decreasing to zero as seen in Fig. 3(b). Although the definition of δ/E_3 may not be as intuitive as δ/V, it incorporates the effect of the thickness of the piezoelectric layer on the electric field. In the case of varying thickness of the piezoelectric layer, it is useful to have the two sensitivities that complement each other.

It can be seen from Eq. (24) that there is a trade-off between the external load P (actuation force) and the tip deflection δ. Appropriate combinations of actuation force and displacement suited to specific applications can be obtained by changing the amplitude of the driving voltage. The external load P (actuation force) at the cantilever tip is plotted against the tip deflection δ in Fig. 4. Both the actuation force and tip deflection increase with the driving voltage when either one of them is constant. For driving voltages ranging from 2 V to 6 V, the maximum actuation force changes from 30 μN to 90 μN. In comparison, a femto slider weighs approximately 6 μN [27]. To displace a femto slider by 10 nm, a driving voltage of about 1V is required.

2.5. Design considerations

The sensitivity and resonant frequency are two most important specifications for actuators. The sensitivity plays an important role in the amplitude of the output, while the resonant frequency together with damping determines the useful frequency range (bandwidth). Ideally, both the sensitivity and resonant frequency are preferred to be as high as possible, however as seen in Fig. 2 a trade-off exists between them. Appropriate combinations are usually chosen based on application requirements.

With a specific interest in enhancing tapping speed of AFM cantilevers, the resonant frequency was selected as the primary design parameter in this study and set to 50 kHz [13, 28]. In addition to a high resonant frequency, tip deflection in the range of 10-100 nm is required. It can be seen from Fig. 2(a) (or calculated from Eq. (5)) that for f_0 = 50 kHz the thickness of silicon t_s is equal to 34 μm. At t_s = 34 μm, the actuation sensitivity is 12.8 nm/V (as seen in Fig. 2(c) or calculated from Eq. (25)). Thus, the driving voltage for the required tip deflection is 1-8 V. This shows the combination of the resonant frequency and sensitivity is suitable for high-speed tapping mode. To let the thicknesses of silicon t_s and ZnO t_p as the only design parameters, the length of the cantilever L and total thickness were set to 1000 μm and 35 μm, respectively. As a result, the piezoelectric ZnO layer is 1 μm thick. The width of the cantilever which is not a variable of f_0 was set to 500 μm. Therefore, the actuator structure consists of a silicon support beam of 1000×500×34 μm^3 and a ZnO thin film of 1 μm thick. The design specifications of the piezoelectric ZnO microcantilever are summarized in Table 2.

3. Fabrication

The piezoelectric ZnO cantilever was fabricated on a p-type (100) silicon wafer by microfabrication. The fabrication process flow is shown in Fig. 5. The fabrication process starts with oxidation of the silicon wafer (Fig. 5(a)). Au/Cr of 100 nm thick is first deposited for the bottom electrode (Fig. 5(b)). ZnO of 1 μm thick is then sputtered at room temperature for the piezoelectric layer (Fig. 5(c)). The optimized process parameters for preparation of the ZnO thin film are listed in Table 3. Characterization results of sputtered ZnO thin films were reported in our previous studies [29]. Following ZnO sputtering, another 100 nm of Au/Cr is deposited for the top electrode (Fig. 5(d)). After deposition of the thin films, the wafer undergoes deep reactive ion etching (DRIE) to carve out the cantilever structure. This is done in two steps. First, the cantilever pattern is defined by etching from the front side (Fig. 5(e)). Second, a cavity is cut from the back side to free the cantilever (Fig. 5(f)). The thickness of the silicon beam is controlled by etching time. The fabricated ZnO cantilever actuator is shown in Fig. 6. The cantilever appears tapered due to nonuniform etching of silicon by DRIE. The thickness at the fixed end measures approximately 36.7 μm, while at the free end 26.6 μm.

4. Characterization

Characterization of the piezoelectric cantilever actuator was performed using a laser Doppler vibrometer (LDV). The experimental setup is shown in Fig. 7. Driving voltage is supplied by a function generator (Agilent 33120A). Tip deflection of the cantilever is captured by the LDV (Polytec). Signals of the driving voltage and tip deflection are processed by a dual channel FFT spectrum analyzer (ONO SOKKI CF-5220Z). Time responses to driving voltages of sinusoid, triangular and square waveforms were investigated. The resonant frequency of the cantilever actuator was identified by an impedance analyzer (Agilent 4294A). Frequency response function was obtained by the spectrum analyzer. Actuation sensitivity, nonlinearity, bandwidth and damping were characterized.

4.1. Time response

To study the dynamic effect on the response of the tip deflection, driving votlage of sinusoid, triangular and square waveforms were applied to the cantilever. Plotted in Fig. 8 are time histories of driving voltage of sine waveform at 20 kHz and the resultant tip deflection. The amplitudes of the driving voltage and tip deflection are 2.764 V and 23 nm, respectively. It is observed in Fig. 8(b) that the peak of the tip deflection trends upward. The phenomenon of displacement drifting is caused by creep which is a viscoelastic behavior associated with piezoelectric materials such as PZT and ZnO [30]. Creep is typically modeled using the generalized Kelvin-Voigt model [31]. Positioning errors induced by creep can be compensated using control techniques [32]. The tip deflection follows the driving voltage well without significant transients. Changing the waveform from sine to triangle resulted in substantial transients in the tip deflection as seen in Fig. 9(b). Fig. 10 shows time response to square wave excitation at 10 kHz. It can be seen in Fig. 10(b) that the tip deflection has larger overshoots than those from the sine and triangle waveforms. Compared with the excitation in Fig. 10(a), the tip deflection hardly settles down, which is attributed to the light damping of the cantilever. To allow the response to reach a steady state, a lower frequency excitation of 400 Hz was applied (Fig. 11). Fig. 11(b) shows that it takes approximately 0.2 msec to damp out the transients. Comparision of the three waveforms shows that in high-speed positioning, sinusoid driving is preferred for reduced impact.

To obtain the actuation sensitivity, the cantilever actuator was excited by sinusoid voltage at 15 kHz. The maximum tip deflection is plotted against the voltage amplitude in Fig. 12. The slope of the fitted line shows that the cantilever actuator has a sensitivity of 12.09 nm/V. The experimental sensitivity is 5.6% lower than the design specification (12.8 nm/V) as shown in Table 2. There are two contributing factors to the discrepancy between the calculated and experimental sensitivities. First, in the modeling the metal thickness (200 nm) is not considered. Omission of the metal electrodes reduces the thickness of the structural layer; hence the stiffness of the cantilever. As a result of a thinner elastic layer, the calculated sensitivity becomes higher (Fig. 2(c)). Second, the fabricated cantilever is tapered with a thicker fixed end (Fig. 6). The variation in thickness causes a higher structural stiffness and thus a lower sensitivity. To address the effect of thickness variation in modeling, the thickness of silicon t_s can be expressed as a function of length $t_s(x)$. Similarly, for cantilevers with variable width, such as triangles, the width b can be replaced by $b(x)$. The response of the tip deflection of the cantilever appears very linear. A transducer's nonlinearity is quantified by [33]

$$\text{Nonlinearity} = \frac{\text{maximum output deviation}}{\text{full scale output}} \tag{27}$$

Nonlinearity of the cantilever actuator was calculated to be 2% full scale.

4.2. Frequency response

Fig. 13 shows the measured resonant frequency of the ZnO cantilever using an impedance analyzer (Agilent 4294A). The fundamental resonance appears at 52.79 kHz, slightly higher than the design specification of 50 kHz. The higher experimental resonant frequency is caused by the same reasons (omission of metal layers in the modeling and thickness variation caused by DRIE etching) behind the lower experimental sensitivity as discussed in Subsection 4.1. Due to the trade-off effect, the

experimental resonant frequency and sensitivity change in opposite directions. To determine the bandwidth of the cantilever actuator, the frequency response fucntion was obtained by the dual channel FFT analyzer. As seen in Fig. 14, the resonant frequency is almost the same as that measured by the impedance analyzer.

The static gain and bandwidth can be obtained from the frequency response function (Fig. 14). Also referred to as sensitivity, the static gain corresponds to the magnitude of the flat region. The bandwidth is determined by the frequency where the static gain deviates by 3 dB [34, 35]. The static gain was found to be 12 nm/V which agrees well with the sensitivity (12.09 nm/V, Fig. 12) obtained in time domain. As shown in Fig. 14, the bandwidth was found to be 27 kHz. The damping ratio of the cantilever actuator can also be calculated using the frequency response function. According to the half-power method, the damping of a system ζ is given by [36]

$$\zeta = \frac{2\Delta f}{f_0} \tag{28}$$

where Δf is the frequency span formed by two frequencies with magnitude 3 dB smaller than the peak (Fig. 15). The damping was calculated to be 0.15% which corresponds to a quality factor Q of 333 in free air. The Q value is about two times bigger than that of a similar cantilever measured 100 nm above the surface [28]. The lower Q value close to the surface is due to squeeze film damping.

5. Conclusions

Analytic formulas for the resonant frequency, actuation sensitivity and force-deflection-voltage behavior of piezoelectric cantilever actuators have been developed. Unlike in previous models where the formulations for deflection and force were given separately, this study presents a unified governing equation which is more convenient to use for actuator design. The resonant frequency and sensitivity were found to be independent of the width of the cantilever. For less power consumption, a wider cross section is preferred for piezoelectric cantilever actuators.

A ZnO microcantilever was designed to operate in the frequency range of 20 kHz which is the desirable bandwidth for the AFM tapping mode [13]. The fabricated ZnO cantilever actuator was characterized for its resonant frequency and actuation sensitivity. The impedance analysis and frequency response function both accurately identified the 1st bending resonance. Time responses to excitations of different waveforms were obtained, and sinusoid driving showed least transient effect. The actuation sensitivity characterized in time domain agreed well with that in the frequency domain. The ZnO cantilever demonstrated good linearity at 15 kHz. For driving voltages ranging from 2 V to 6 V, the maximum tip deflection and actuation force can reach 60 nm and 90 μN, respectively. The specifications of the ZnO microcantilever also suit applications such as flying height control of magnetic head sliders in hard disk drives, which demands nanopositioning of a mass (0.6 mg) at frequencies up to 15 kHz [37, 38].

References

[1] T. Morita, Miniature piezoelectric motors, Sensors and Actuators A: Physical 103 (2003) 291-300.

[2] Y. Miyahara, M. Deschler, T. Fujii, S. Watanabe, H. Bleuler, Non-contact atomic force microscope with a PZT cantilever used for deflection sensing, direct oscillation and feedback actuation, Applied Surface Science 188 (2002) 450-455.

[3] C. Kugeler, A. Hennings, U. Bottger, R. Waser, An integrated microelectromechanical microwave switch based on piezoelectric actuation, Journal of Electroceramics 22 (2009) 145-149.

[4] W.H. Tu, K. Chang, Piezoelectric transducer-controlled dual-mode switchable bandpass filter, IEEE Microwave and Wireless Components Letters 17 (2007) 199-201.

[5] G.K. Lau, H.J. Du, A piezoelectric quad-morph actuated suspension for hard disk drives, Journal of Micromechanics and Microengineering 16 (2006) 1833-1840.

[6] T. Ikeda, Fundamentals of piezoelectricity, Oxford University Press, Oxford, 1990, p. 222.

[7] T. Xu, G.Y. Wu, G.B. ZHang, Y.L. Hao, The compatibility of ZnO piezoelectric film with micromachining process, Sensors and Actuators A: Physical 104 (2003) 61-67.

[8] T. Itoh, T. Suga, Scanning force microscope using a piezoelectric microcantilever, Journal of Vacuum Science and Technology B 12 (1994) 1581-1585.
[9] T. Itoh, T. Suga, Piezoelectric force sensor for scanning force microscopy, Sensors and Actuators A: Physical 43 (1994) 305-310.
[10] T. Itoh, T. Suga, Self-excited force-sensing microcantilevers with piezoelectric thin films for dynamic scanning force microscopy, Sensors and Actuators A: Physical 54 (1996) 477-481.
[11] T. Itoh, T. Ohashi, T. Suga, Noncontact scanning force microscopy using a direct-oscillating piezoelectric microcantilever, Journal of Vacuum Science and Technology B 14 (1996) 1577-1581.
[12] S.R. Manalis, S.C. Minne, C.F. Quate, Atomic force microscopy for high speed imaging using cantilevers with an integrated actuator and sensor, Applied Physics Letters 68 (1996) 871-873.
[13] S.C. Minne, G. Yaralioglu, S.R. Manalis, J.D. Adams, J. Zesch, A. Atalar, C.F. Quate, Automated parallel high-speed atomic force microscopy, Applied Physics Letters 72 (1998) 2340-2342.
[14] T. Shibata, K. Unno, E. Makino, Y. Ito, S. Shimada, Characterization of sputtered ZnO thin film as sensor and actuator for diamond AFM probe, Sensors and Actuators A: Physical 102 (2002) 106-113.
[15] J. Vazquez, P. Sanz, J.L. Sanchez-Rojas, Behaviour of forbidden modes in the impedance characterization and modeling of piezoelectric microcantilevers, Sensors and Actuators A: Physical 136 (2007) 417-425.
[16] S.N. Mahmoodi, M.F. Daqaq, N. Jalili, On the nonlinear-flexural response of piezoelectrically driven microcantilever sensors, Sensors and Actuators A: Physical 153 (2009) 171-179.
[17] Q.M. Wang, L.E. Cross, Performance analysis of piezoelectric cantilever bending actuators, Ferroelectrics 215 (1998) 187-213.
[18] D.L. DeVoe, A.P. Pisano, Modeling and optimal design of piezoelectric cantilever microactuators, Journal of Microelectromechanical Systems 6 (1997) 266-270.
[19] S. Timoshenko, Analysis of bi-metal thermostats, Journal of the Optical Society of America and Review of Scientific Instruments 11 (1925) 233-255.
[20] M.R. Steel, F. Harrison, P.G. Harper, The piezoelectric bimorph: An experimental and theoretical study of its quasistatic response, Journal of Physics D: Applied Physics 11 (1978) 979-989.
[21] J.G. Smits, W.S. Choi, The constituent equations of piezoelectric heterogeneous bimorphs, IEEE Transactions on Ultrasonic, Ferroelectrics and Frequency Control 38 (1991) 256-270.
[22] L. Meirovitch, Fundamentals of vibrations, McGraw-Hill, Boston, 2001, p. 403.
[23] J.M. Gere, Mechanics of materials, 6th ed., Brooks/Cole-Thomas Learning, Belmont, CA, 2004, p. 403.
[24] C. Jagadish, S.J. Pearton, Zinc oxide bulk, thin films and nanostructures: processing, properties and applications, Elsevier, Amsterdam ; Boston, 2006, p. 445.
[25] K.E. Petersen, Silicon as a Mechanical Material, Proceedings of the IEEE 70 (1982) 420-457.
[26] Q.M. Wang, L.E. Cross, Tip deflection and blocking force of soft PZT-based cantilever RAINBOW actuators, Journal of the American Ceramic Society 82 (1999) 103-110.
[27] B. Liu, M.S. Zhang, S.K. Yu, L. Gonzaga, Y.S. Ho, H.F. Xu, Femto slider: Fabrication and evaluation, IEEE Transactions on Magnetics 39 (2003) 909-914.
[28] T. Sulchek, R. Hsieh, J.D. Adams, G.G. Yaralioglu, S.C. Minne, C.F. Quate, J.P. Cleveland, A. Atalar, D.M. Adderton, High-speed tapping mode imaging with active Q control for atomic force microscopy, Applied Physics Letters 76 (2000) 1473-1475.
[29] P.H. Wang, H.J. Du, S.N. Shen, M.S. Zhang, B. Liu, Preparation and characterization of ZnO microcantilever for nanoactuation, Nanoscale Research Letters 7 (2012) 1-5.
[30] H.M.S. Georglou, R. Mrad, Dynamic electromechanical drift model for PZT, Mechatronics, 18 (2008) 81-89.
[31] R.J. Wood, E. Steltz, R.S. Fearing, Nonlinear performance limits for high energy density piezoelectric bending actuators, in: IEEE International Conference on Robotics and Automation, 2005, pp. 3633-3640.
[32] D. Croft, G. Shed, S. Devasia, Creep, hysteresis, and vibration compensation for piezoactuators: Atomic force microscopy application, Journal of Dynamic Systems Measurement and Control-Transactions of the ASME 123 (2001) 35-43.
[33] J.P. Bentley, Principles of measurement systems, Longman, London; New York, 1983, p. 7.
[34] C.W. De Silva, Mechatronics: an integrated approach, CRC Press, Boca Raton, 2005, p. 431.
[35] C.-C. Wu, C.-C. Lee, G.Z. Cao, I.Y. Shen, Effects of corner frequency on bandwidth and resonance amplitude in designing PZT thin-film actuators, Sensors and Actuators, A: Physical 125 (2006) 178-185.
[36] A.G. Piersol, T.L. Paez, C.M. Harris, Harris' shock and vibration handbook, 5th ed., McGraw-Hill, New York, 2002, p. 2.18.
[37] Y.F. Li, R. Horowitz, R. Evans, Vibration control of a PZT actuated suspension dual-stage servo system using a PZT sensor, Transactions on Magnetics 39 (2003) 932-937.

[38] H. Du, G.K. Lau, B. Liu, Actuated suspensions with enhanced dynamics for hard disk drives, IEEE Transactions on Magnetics 41 (2005) 2887-2889.

Biographies

Yanhui Yuan received his B. Eng in mechanical engineering and M. Eng in electrical engineering from Chongqing University, China in 1997 and 2001, respectively. In 2010, he earned a PhD degree in mechanical engineering from Nanyang Technological University, Singapore and became a lecturer in UESTC, Zhongshan, China. Dr. Yuan is currently a research fellow in Center for Mechanics of Microsystems, Nanyang Technological University. His research interests are MEMS transducers.

Hejun Du obtained both his B. Eng and M. Eng from Nanjing University of Aeronautics and Astronautics, China in 1983 and 1986, respectively. Subsequently, he lectured there until 1988 before he left for Imperial College of Science, Technology and Medicine, UK for his Ph.D. study. Du Hejun joined Nanyang Technological University (NTU), Singapore in 1991 after obtaining Ph.D. He is currently an Associate Professor in the School of Mechanical and Aerospace Engineering, NTU, Singapore. Dr. Du's research interests mainly include three areas: (1) numerical and computational methods for engineering applications; (2) MEMS sensors and actuators; (3) smart materials and their engineering applications.

List of Table

Material	E (GPa)	ρ (kg/m^3)	d_{31} (C/N)
ZnO	210	5750	-5.43×10^{-12}
Silicon	190	2329	N.A.

Table 1

Specifications	Value
Resonant frequency (f_0) (kHz)	50
Sensitivity (nm/V)	12.8
Thickness of ZnO (μm)	1
Thickness of silicon (μm)	34
Length of cantilever (μm)	1000
Width of cantilever (μm)	500

Table 2

Conditions and parameters	Value
Target	ZnO (99.99%)
Substrate	Silicon (100)
Target-substrate distance (mm)	70
RF power (W)	90
Substrate temperature	Room temperature
O_2 (sccm)	2
Ar (sccm)	6
Working pressure (Pa)	0.8
Deposition rate (nm/h)	300

Table 3

List of Figure

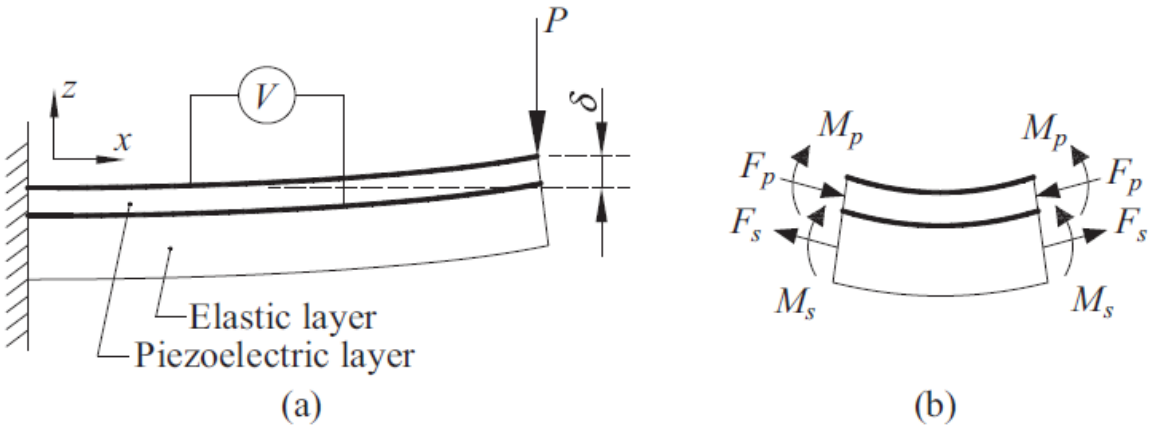
P
z
x
V
δ
Elastic layer
Piezoelectric layer
(a)
M_p
M_p
F_p
F_p
F_s
F_s
M_s
M_s
(b)

Fig. 1

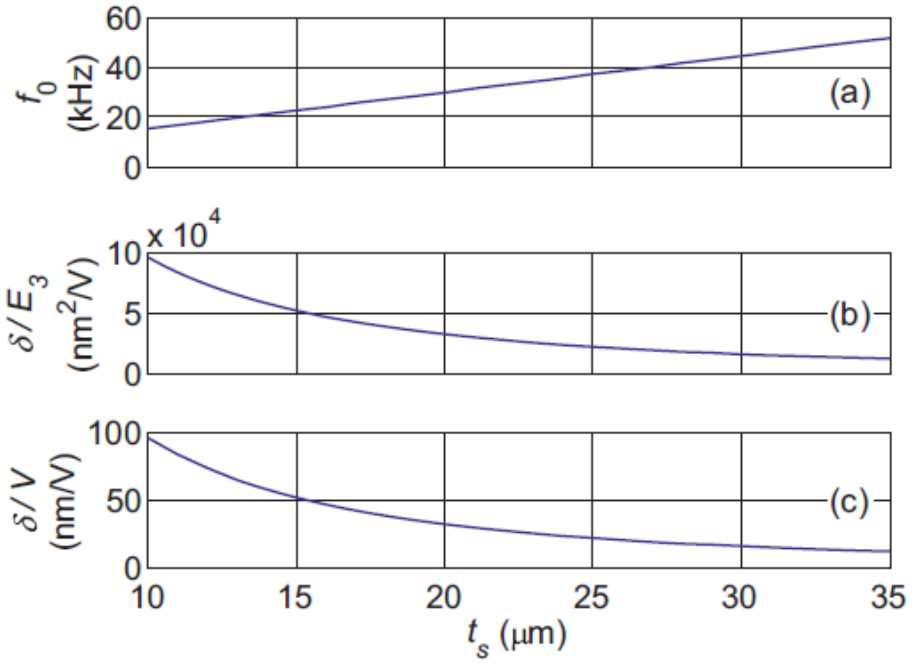
60
40
20
0
f_0 (kHz)
(a)
x 10^4
10
5
0
δ / E_3 (nm^2/V)
(b)
100
50
0
δ / V (nm/V)
(c)
10
15
20
25
30
35
t_s (μm)

Fig. 2

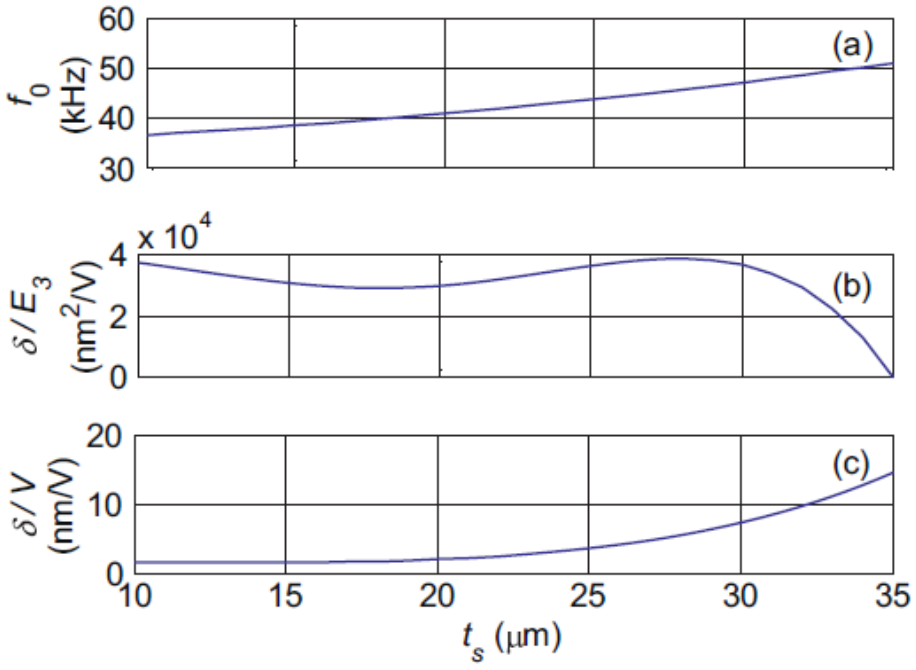
60
50
40
30
f_0 (kHz)
(a)
x 10^4
4
2
0
δ / E_3 (nm^2/V)
(b)
20
10
0
δ / V (nm/V)
(c)
10
15
20
25
30
35
t_s (μm)

Fig. 3

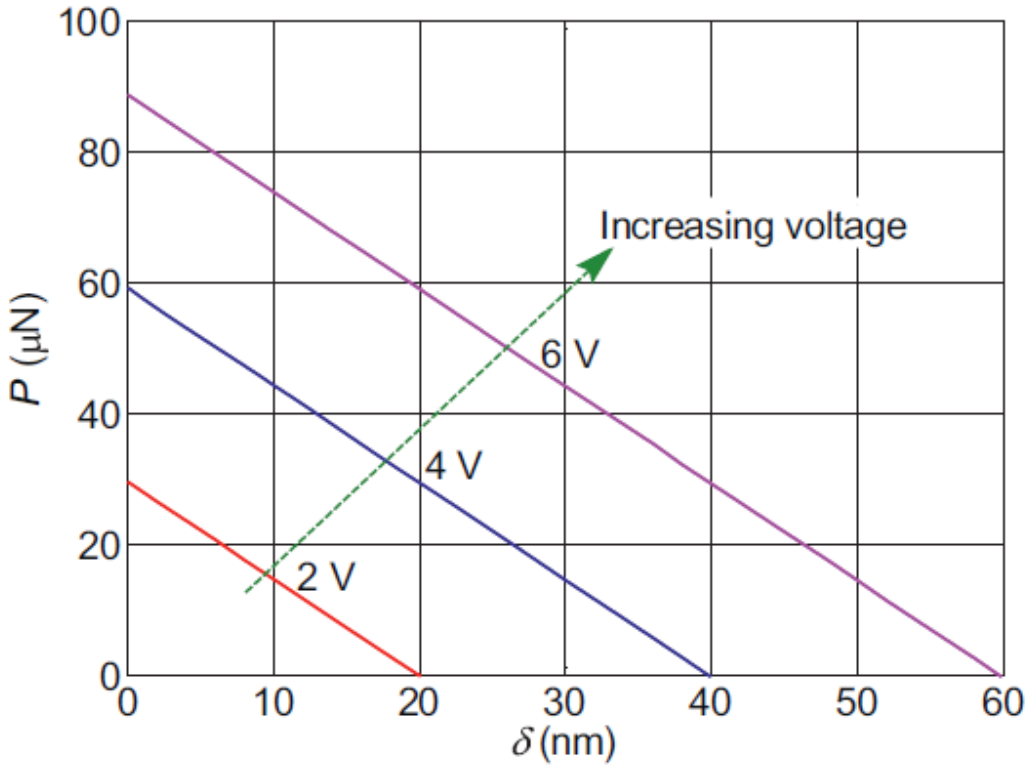
100
80
60
40
20
0
P (μN)
0
10
20
30
40
50
60
δ (nm)
Increasing voltage
6 V
4 V
2 V

Fig. 4

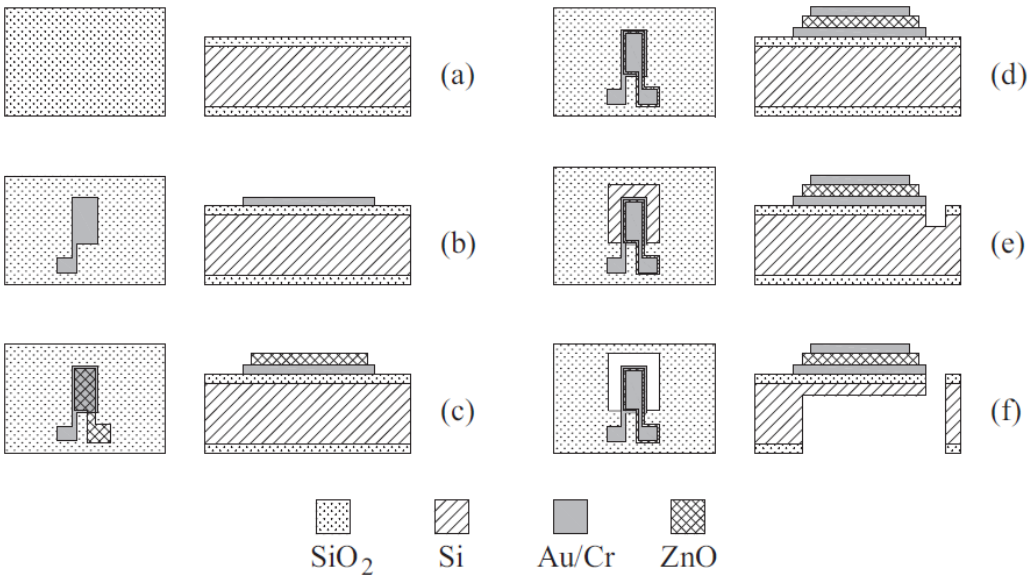

Fig. 5

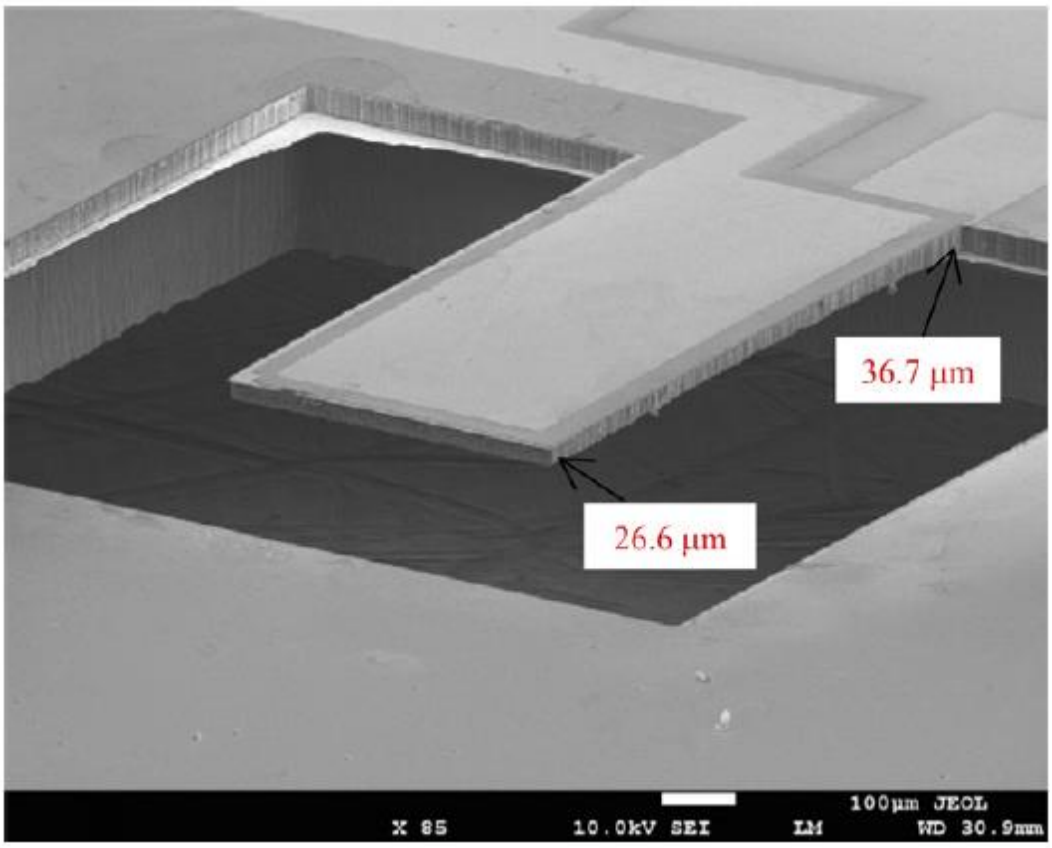

Fig. 6

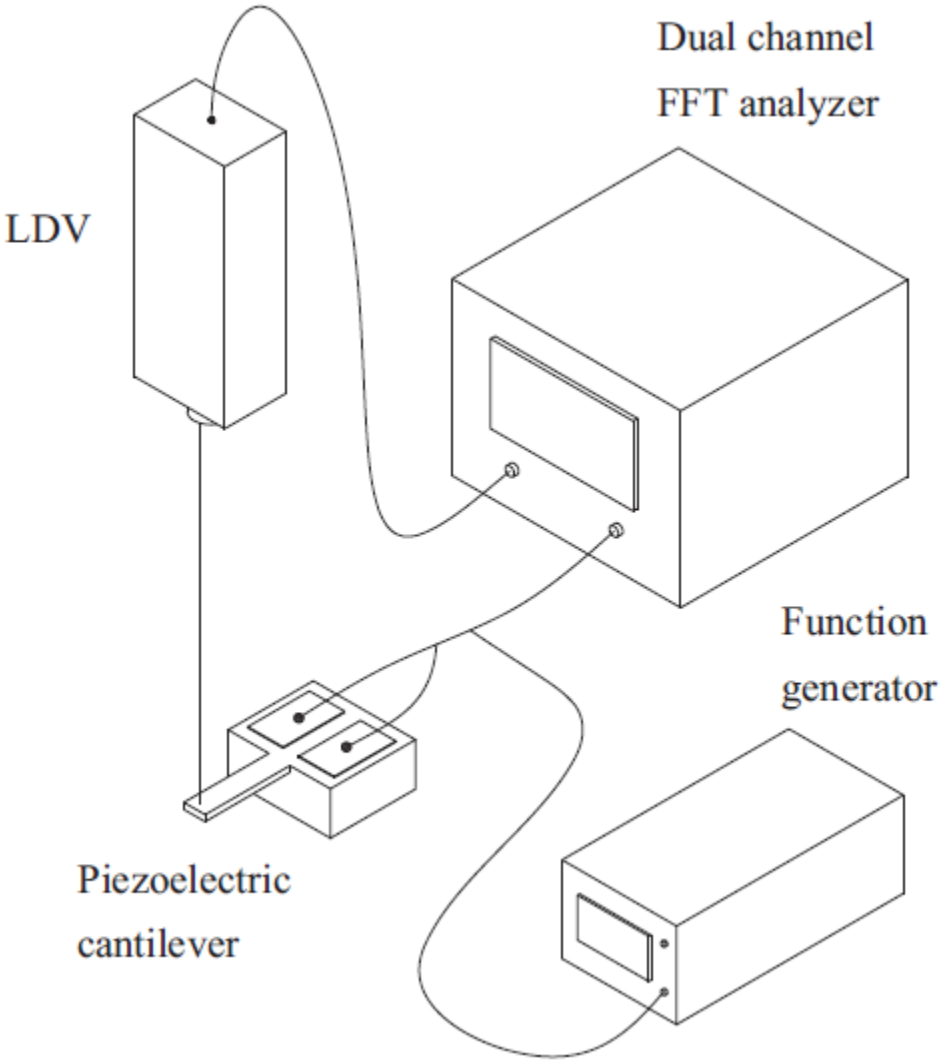
Dual channel
FFT analyzer
LDV
Function
generator
Piezoelectric
cantilever

Fig. 7

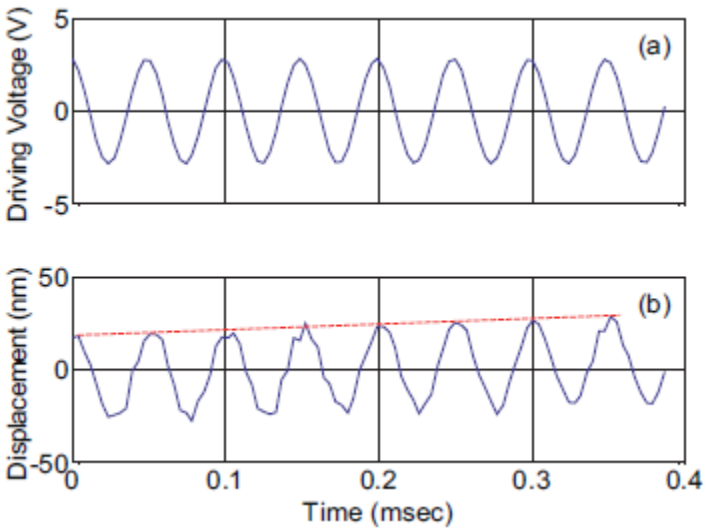
Driving Voltage (V)
5
0
-5
(a)
Displacement (nm)
50
0
-50
(b)
0
0.1
0.2
0.3
0.4
Time (msec)

Fig. 8

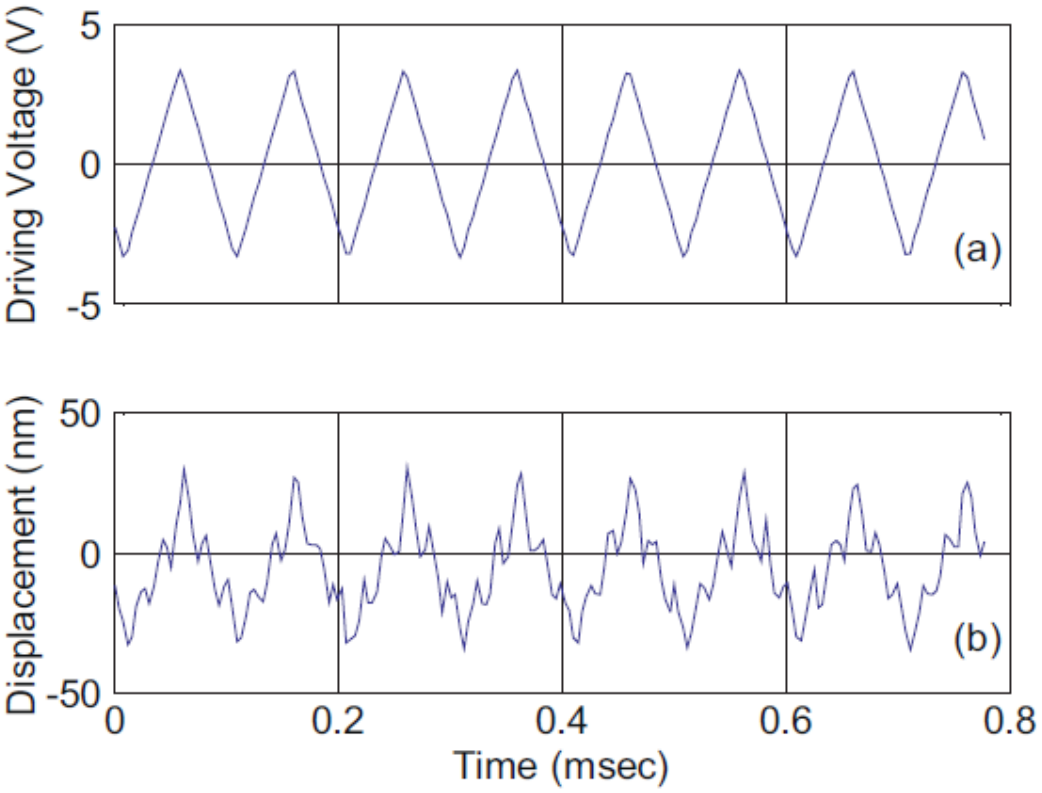
Driving Voltage (V)
5
0
-5
(a)
Displacement (nm)
50
0
-50
(b)
0
0.2
0.4
0.6
0.8
Time (msec)

Fig. 9

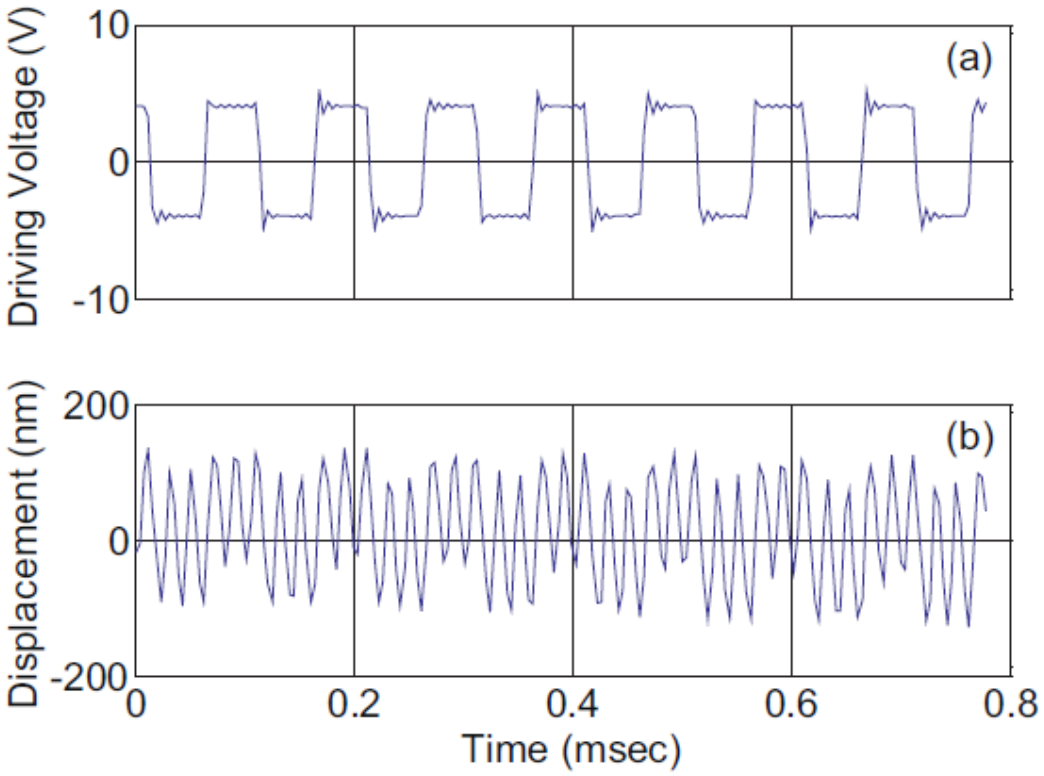
Driving Voltage (V)
10
0
-10
(a)
Displacement (nm)
200
0
-200
(b)
0
0.2
0.4
0.6
0.8
Time (msec)

Fig. 10

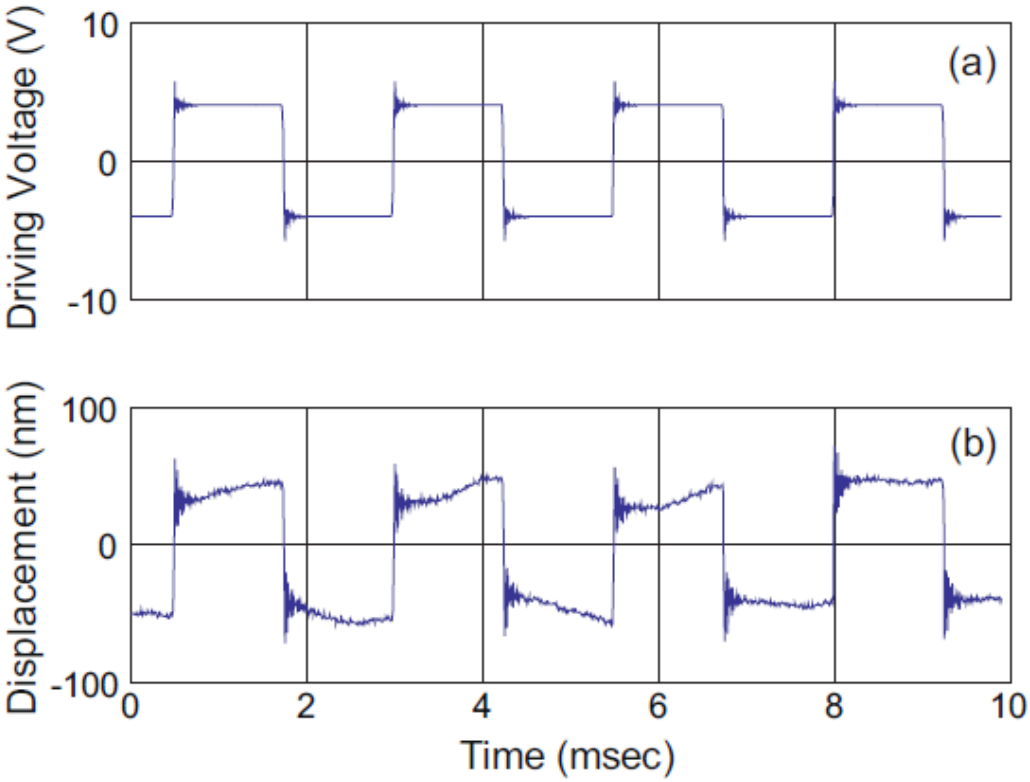
Driving Voltage (V)
10
0
-10
(a)
Displacement (nm)
100
0
-100
(b)
0
2
4
6
8
10
Time (msec)

Fig. 11

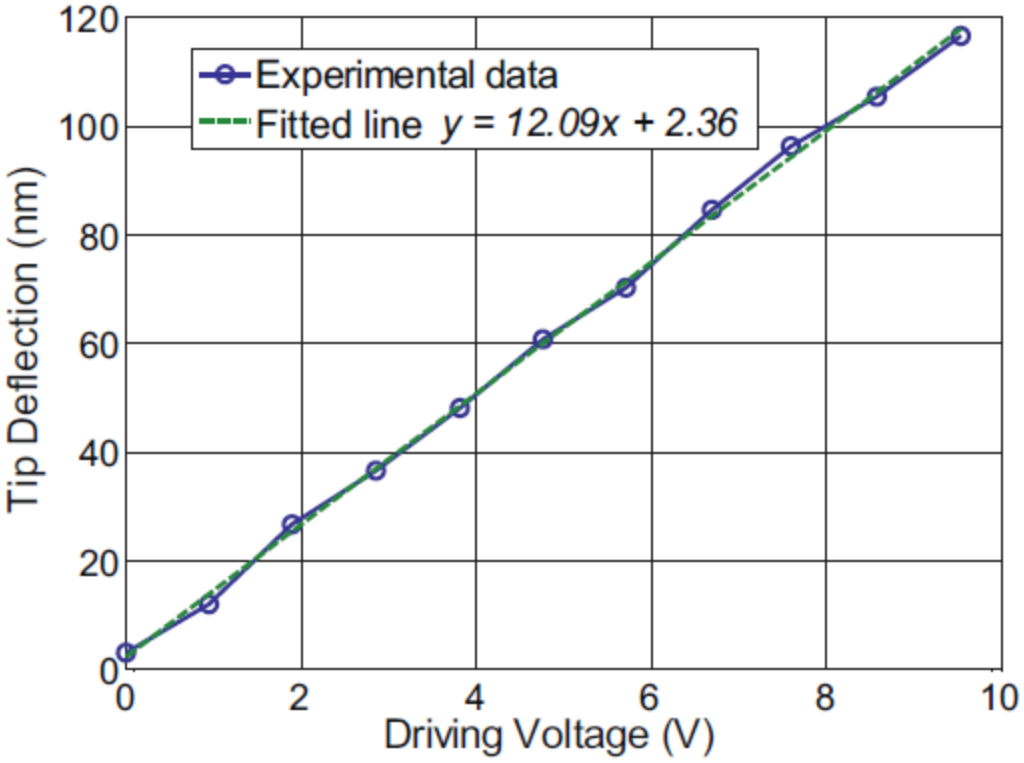
Experimental data
Fitted line y = 12.09x + 2.36
Tip Deflection (nm)
Driving Voltage (V)
0
20
40
60
80
100
120
0
2
4
6
8
10

Fig. 12

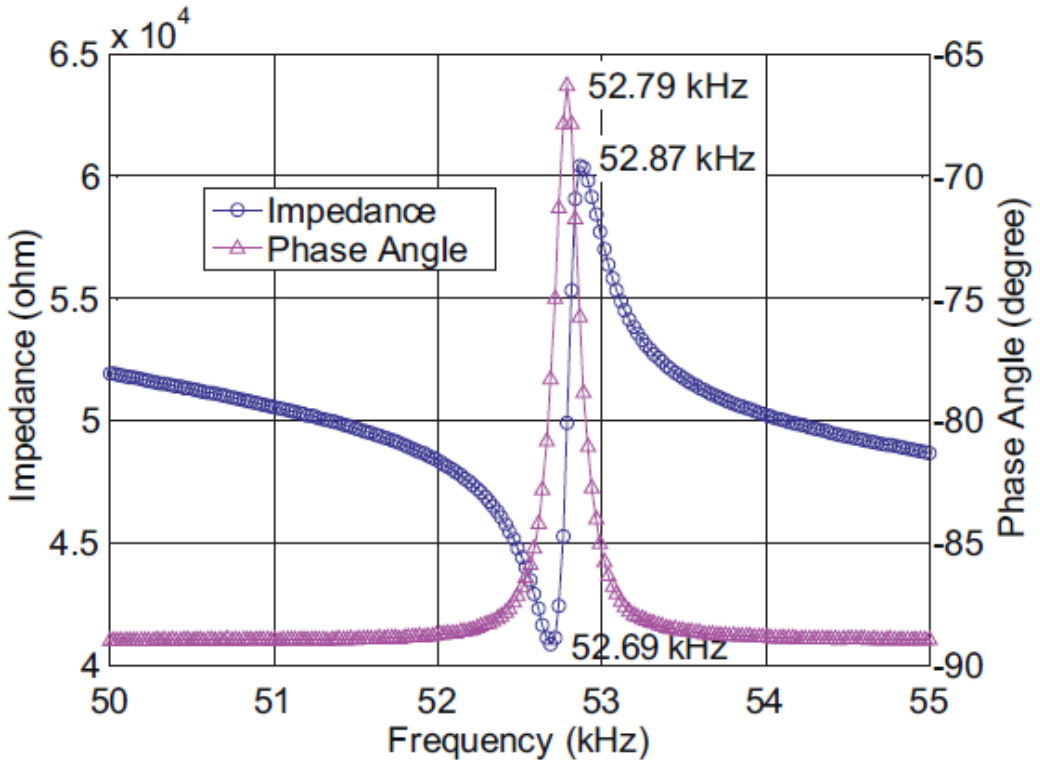
x 10^4
6.5
6
5.5
5
4.5
4
-65
-70
-75
-80
-85
-90
50
51
52
53
54
55
Impedance (ohm)
Phase Angle (degree)
Frequency (kHz)
Impedance
Phase Angle
52.79 kHz
52.87 kHz
52.69 kHz

Fig. 13

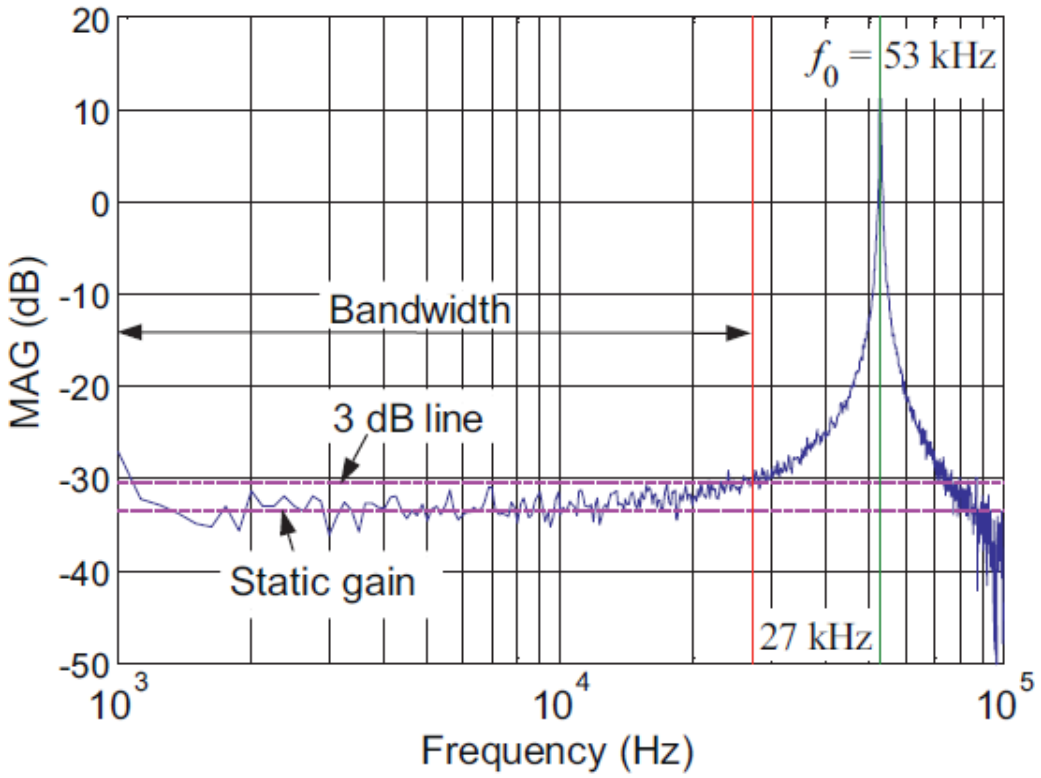
20
10
0
-10
-20
-30
-40
-50
MAG (dB)
f_0 = 53 kHz
Bandwidth
3 dB line
Static gain
27 kHz
10^3
10^4
10^5
Frequency (Hz)

Fig. 14

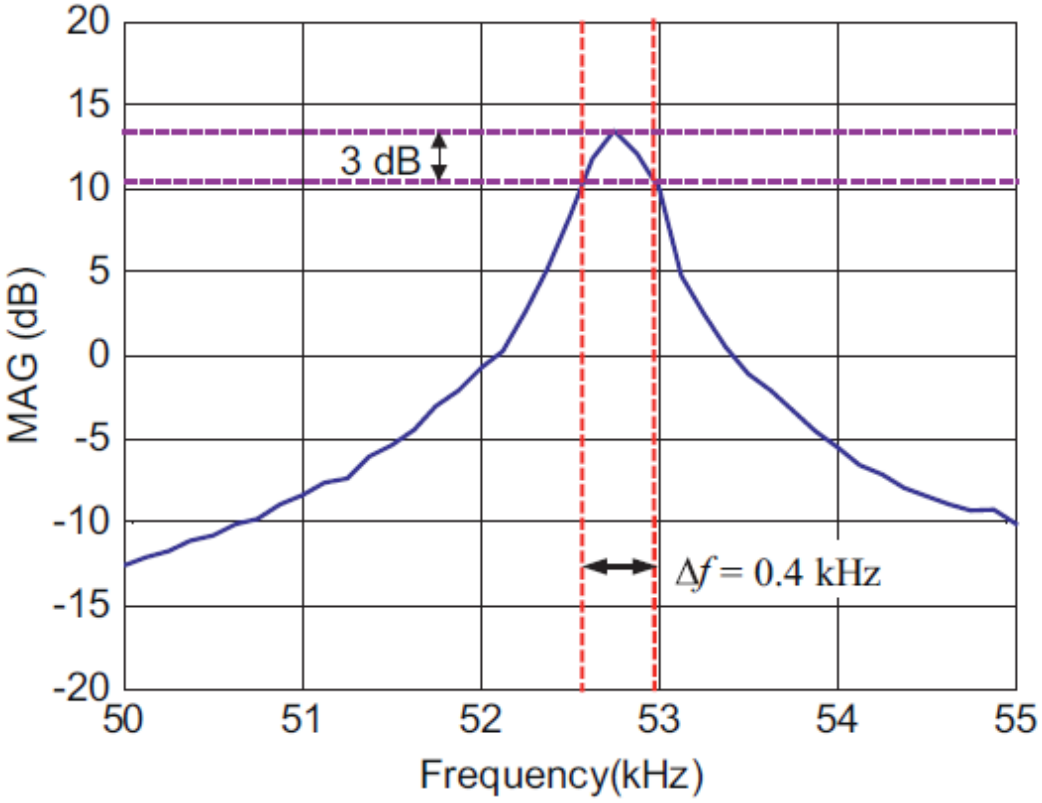
20
15
10
5
0
-5
-10
-15
-20
MAG (dB)
3 dB
Δf = 0.4 kHz
50
51
52
53
54
55
Frequency(kHz)

Fig. 15